Persistent entanglement of valley exciton qubits in transition metal dichalcogenides integrated into a bimodal optical cavity

Halyne S. Borges ®,[1] Celso A. N. Júnior ®,[2] David S. Brandão ®,[2] Fujun Liu ®,[2] V. V. R. Pereira ®,[2] S. J. Xie,[3] Fanyao Qu ®,[2,4] and A. M. Alcalde ®[5]

[1]*Instituto Federal do Triângulo Mineiro, Patrocínio MG, 38747-792, Brazil*
[2]*Instituto de Física, Universidade de Brasília, Brasília-DF 70919-970, Brazil*
[3]*School of Physics, State Key Laboratory of Crystal Materials, Shandong University, Jinan 250100, China*
[4]*International Center for Physics, University of Brasília, 70910-900, Brasília, Brazil*
[5]*Instituto de Física, Universidade Federal de Uberlândia, 38400-902 Uberlândia, MG, Brazil*

We report dissipative dynamics of two valley excitons residing in the K and K' valleys of a bare WSe$_2$ monolayer and the one being integrated into a bimodal optical cavity. In the former, only when the exciton-field detunings in the K and K' valleys are rigorously equal (resonant detuning) can partially entangled stationary states be created. Otherwise, the concurrence of exciton qubits turns to zero. Remarkably, in the latter (the WSe$_2$ monolayer in a bimodal optical cavity), the transfers of entanglement from one subsystem (exciton/light) to the other (light/exciton) take place. Hence a finite stationary concurrence of exciton qubits is always generated, independent of whether the exciton-field detuning in two valleys is resonant or nonresonant. In addition, it can even reach as high as 1 (maximally entangled state of two valley excitons). Since there no real system which has a strictly resonant detuning, an immersion of the WSe$_2$ monolayer in a bimodal optical cavity provides an opportunity to overcome the challenge facing by the bare WSe$_2$, opening a novel realm of potential qubits.

I. INTRODUCTION

Monolayer transition metal dichalcogenides (TMDs), denoted by MX$_2$ with M = Mo, W, and X = S, Se, possess a broken inversion symmetry which leads to a direct band gap at two degenerate but inequivalent valleys, K and K' [1,2]. Although these two states are energetically degenerate, the orbital angular momentum quantum number of the valence band (VB) in the K valley is $+2$, whereas it is -2 in the K' valley. Moreover, the strong spin-orbit coupling splits the band edge states, resulting in an energy separation between spin-up and spin-down states reaching 0.45 eV in the VB and tens of meV in the conduction band (CB) of monolayer WX$_2$ [2]. In addition, time-reversal symmetry preservation of the TMDs requires that the spin splitting in different valleys must be opposite [3,4]. As a result, the spin-down (spin-up) state in the K valley would have the same energy with its corresponding spin-up (spin-down) state in the K' valley, see Fig. 1. These characteristics of the monolayer TMDs lead to so-called spin-valley locking and valley-dependent optical selection rules [3,5]. In turn, when the electrons recombine to the holes in the K (K') valley, they can only generate left (right) circularly polarized light [2,3,5]. Furthermore, because of spin-valley locking, the intervalley scattering happens only when the intervalley spin flips and the large momentum transfer ($\approx K - K'$) simultaneously occur. This criteria strongly suppresses the intervalley scatterings, endowing a long valley polarization time of the carriers [5]. Recently, quantum coherence of valleys has been experimentally demonstrated [3], and

coherent control of valley-spin qubits has also been theoretically proposed [6,7]. Therefore the valley of the monolayer TMDs has the potential to be used as quantum information carriers.

Owing to the two-dimensional (2D) spatial confinement and reduced dielectric screening, the monolayer TMDs exhibit strong Coulomb interactions [5,8–10]. Under light excitation, the formation of tightly bound electron-hole pairs, so-called excitons, is favored [4,8,9,11]. Owing to optical valley selectivity, namely the right-handed (left-handed) circularly polarized light, only creates the excitons in $K(K')$ valley, the excitons will be endowed with a valley degree of freedom, denominated as valley excitons. In addition, their high binding energies of up to a few hundred meV make excitons quite stable, even at room temperature [9,12,13]. It sheds light on room-temperature valley exciton qubits.

The field of quantum computing was first foreseen by Richard Feynman in the early 1980s with the aim of solving quantum mechanics problems. Since then, the interest of both fundamental-science researchers and industrial actors, like Google, IBM, Intel, and Lockheed Martin, has increased exponentially in this field. Many qubits, the fundamental building block of a quantum computer, such as electronic spin [14], nuclear spin, electronic states of trapped ions, superconducting qubit, and topological qubit, have been proposed and explored. Although great progress in quantum computing has been made in recent years, such as increasing processing velocity, it still faces challenges. For example, the ion qubit

needs to be in a high vacuum, the superconducting qubit has a short decoherence time and must be kept very cold (below 100 mK or 0.1° above absolute zero), etc. To shed light on overcoming these challenges, we propose another alternative: valley exciton qubits implemented in TMDs. The large thermal stability, long valley coherence times combining with fast and conveniently operation by circularly polarized laser field make valley exciton a great compromising quantum information carrier. It is worth recalling that the quantum qubit based on valley degree of freedom has been previously addressed in double quantum dot systems based on graphene [15] or single-layer TMDs [14], where the electron spin valleys are proposed as controllable qubits.

In this work, we focus on the study of quantum entanglement of intervalley excitonic states, and special interest is devoted to the optical generation of entanglement and the injection of excitonic entanglement into the system and its availability over long time periods for applications in quantum information processing. The concurrence which is used to measure entanglement of valley excitons, however, always comes down to a vanishing small value for a nonresonant detuning (exciton-field detuning in valley K is different from that in K'). Interestingly, the situation is changed for the TMDs integrated into a bimodal optical cavity. By tuning the initial state of the system, exciton-field detunings, the electron-hole exchange interaction (EXI), and the coupling between exciton and cavity mode, the concurrence of two exciton qubits can remarkably reach as high as 1. This is attributed to cavity-enhanced light-matter interaction. These results demonstrate the viability and tunability of valley exciton qubits which possess high-speed operation, easy and convenient control, long coherence time, and capability of working at room temperature.

II. THEORETICAL FRAMEWORK

Here we chose tungsten diselenide (WSe_2) as the physical system for quantum entanglement implementation. The band structure and wave functions of WSe_2 are obtained by density-functional theory calculations using the QUANTUM ESPRESSO package [16] (see Fig. 2). The kinetic energies cutoff for wave function (ecutwfc) and charge density (ecutrho) are set as 600 and 60 Ry, respectively. The range-separated hybrid functional proposed by Heyd, Scuseria, and Ernzerhof (HSE06) [17,18] is adopted for the exchange-correlation energy. Numerical integrations in the Brillouin zone are evaluated with the Monkhorst-Pack mesh of $12 \times 12 \times 1$. All structures are relaxed until the total energy converges to within 10^{-4} eV during the self-consistent loop, employing the Methfessele-Paxton method. To correctly account for the strong spin-orbit coupling arising from heavy tungsten atoms in WSe_2 [9,11], the spin-orbit coupling corrections were included in the electronic property calculations.

With the obtained energies and wave functions, we develop a tight-binding (TB) model using the package Wannier90 [19]. This maps the ground-state wave functions from the density-functional theory output file onto a maximally localized Wannier function basis $\{|W_{i\mathbf{R}}\rangle\}$, where $i = (I, \alpha)$ is the composite index of the atomic orbit α of a atom with atom
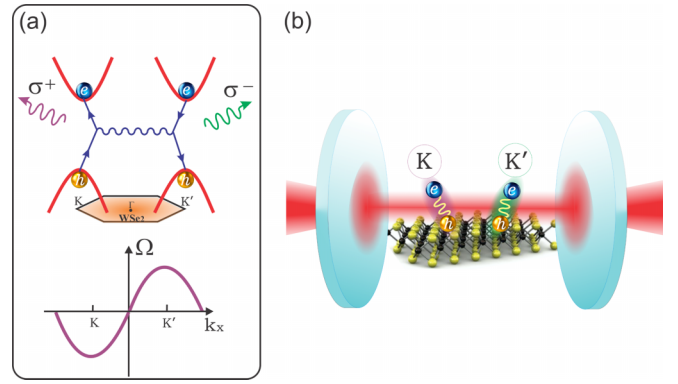
FIG. 1. (a) Upper part: Schematic diagram of Brillouin zone (filled hexagonal), valley excitons formation, and Feynman diagram of EXI (lines with arrows); lower part: Berry curvature of the lowest conduction band in K and K' valleys and (b) TMD integrated nanocavity system.

site $\mathbf{r}_I$. $\mathbf{R} = R_a \mathbf{a} + R_b \mathbf{b} + R_c \mathbf{c}$ is the Bravais lattice vector with $R_{a/b/c}$ being the Bravais lattice vector component on the direction of the unit cell lattice vector $\mathbf{a}/\mathbf{b}/\mathbf{c}$. The basis function of TB model is thus given by

$$|\phi_{i\mathbf{k}}\rangle = \frac{1}{\sqrt{N}} \sum_{\mathbf{R}} e^{-i\mathbf{k}\cdot\mathbf{R}} |W_{i\mathbf{R}}\rangle, \qquad (1)$$

and elements of the TB Hamiltonian $\mathbf{H}^{TB}$ are given by

$$\mathbf{H}_{ij}^{TB}(\mathbf{k}) = \sum_{\mathbf{R}} e^{-i\mathbf{k}\cdot\mathbf{R}} t_{ij}(\mathbf{R}), \qquad (2)$$

where $t_{ij}(\mathbf{R}) = \langle W_{i0}|H_{KS}|W_{j\mathbf{R}}\rangle$ is the matrix element extracted from the Wannier90 output file, with H_{KS} being the Hamiltonian of Kohn-Sham equation. In the following, we utilize the output of TB model calculation as an input to get the values of exciton energy and its radiation lifetime.
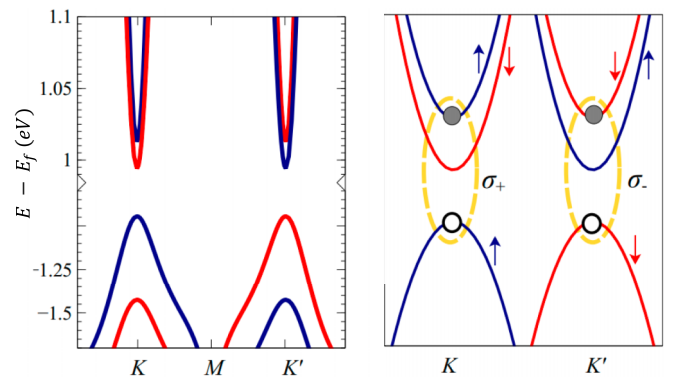
FIG. 2. (a) Band structure of monolayer WSe2 nearby K and K' points and (b) schematic representation of valley bright exciton formations. Red and blue curves correspond to spin-up and spin-down states, respectively.

III. VALLEY EXCITON IN WSe₂ MONOLAYER

A. Bethe-Salpeter equation for valley exciton

With eigenvalues and wave functions of the single particle at hand, we can calculate excitonic states through many-body problem using the Bethe-Salpeter equation. The exciton Hamiltonian is composed of the electron H_e and the hole H_h single-particle Hamiltonians plus Coulomb interaction $V_{\vec{R}}$ which couples the electron-hole pairs,

$$H_X = H_e + H_h + V_{\mathbf{R}}. \tag{3}$$

Due to the finite width of the TMD monolayer and the spatial inhomogeneity of the dielectric screening environment, we choose to modeling the interaction Coulomb potential, using the Keldysh formalism [8],

$$V_{\mathbf{R}} = -\frac{e^2}{8\epsilon_0\epsilon_d r_0}\left[H_0\left(\frac{|\mathbf{R}|}{r_0}\right) - Y_0\left(\frac{|\mathbf{R}|}{r_0}\right)\right], \tag{4}$$

where H_0 and Y_0 are the Struve and Bessel functions of the second kind, respectively; ϵ_d is the effective dielectric constant ($\epsilon_d = 2.39$ for a SiO_2 substrate); and r_0 represents a characteristic length, defined by $r_0 = 2\pi\chi_{2D}/\epsilon_d$, with χ_{2D} being the two-dimensional polarizability.

Since we study periodic lattices, it is more convenient to work in the reciprocal space; in k space the Keldysh potential acquires the form [8,9]

$$V_{\mathbf{q}} = -\frac{e^2}{2\epsilon_0\epsilon_d|\mathbf{q}|(1 + r_0|\mathbf{q}|)}, \tag{5}$$

where $\mathbf{q} = \mathbf{k} - \mathbf{k}'$. It is worth noting that a controllable tuning of the band gap and the exciton binding energy can be realized by engineering the dielectric environment of the monolayer, e.g., by encapsulating the TMDC between other layered materials or modifying the substrate.

An exciton state $|\Psi_S(\mathbf{Q})\rangle$ is a coherent superposition of hole (with crystal momentum $\mathbf{k}$) and electron (with crystal momentum $\mathbf{k} + \mathbf{Q}$) states from band pairs (v, c) in the reciprocal space and can be written as

$$|\Psi_S(\mathbf{Q})\rangle = \sum_{c,v,\mathbf{k}} A^S_{c,v,\mathbf{k},\mathbf{Q}}|c, \mathbf{k} + \mathbf{Q}\rangle \otimes |v, \mathbf{k}\rangle, \tag{6}$$

where S and $\mathbf{Q}$ are the exciton band index and the center-of-mass momentum, respectively. In this study, we focus on the low-energy excitons. Thus we only consider the two highest VBs and the two lowest CBs. The exciton eigenvalue problem in the basis displayed in Eq. (6) leads to the following Bethe-Salpeter equation:

$$E_S(\mathbf{Q})A^S_{c,v,\mathbf{k},\mathbf{Q}} = (E_{c,\mathbf{k}+\mathbf{Q}} - E_{v,\mathbf{k}})\delta_{(\mathbf{k},v,c),(\mathbf{k}',v',c')}A^S_{c,v,\mathbf{k},\mathbf{Q}}$$
$$+ \frac{1}{A}\sum_{k',v',c'} W_{(\mathbf{k},v,c),(\mathbf{k}',v',c'),\mathbf{Q}}\, A^S_{c',v',\mathbf{k}',\mathbf{Q}}. \tag{7}$$

In the equation above, $A = A_c N_k^2$ is the total area of the crystal, where $A_c = \sqrt{3}a^2/2$ and a is the lattice constant. Furthermore, $W_{(\mathbf{k},v,c),(\mathbf{k}',v',c'),\mathbf{Q}}$ represents the matrix element of the many-body Coulomb potential including direct W^d and exchange W^x terms, and $E_S(\mathbf{Q})$ is the exciton energy of the Sth state with the center-of-mass momentum $\mathbf{Q}$.

To simplify the calculation, we apply the Tamm-Dancoff approximation to the many-body Coulomb potential, which neglects the orbital character of the Coulomb interaction. In this case $W^d_{(\mathbf{k},v,c),(\mathbf{k}',v',c'),\mathbf{Q}}$ and $W^x_{(\mathbf{k},v,c),(\mathbf{k}',v',c'),\mathbf{Q}}$ are given by

$$W^d_{(\mathbf{k},v,c),(\mathbf{k}',v',c'),\mathbf{Q}} = V_{\mathbf{k}-\mathbf{k}'}\langle c, \mathbf{k} + \mathbf{Q}|c', \mathbf{k}' + \mathbf{Q}\rangle \langle v, \mathbf{k}|v', \mathbf{k}'\rangle \tag{8}$$

and

$$W^x_{(\mathbf{k},v,c),(\mathbf{k}',v',c'),\mathbf{Q}} = V_{\mathbf{Q}}\langle c, \mathbf{k} + \mathbf{Q}|v, \mathbf{k}\rangle \langle v', \mathbf{k}'|c', \mathbf{k}' + \mathbf{Q}\rangle. \tag{9}$$

Equation (9) indicates that for $Q = 0$, the exchange interaction is equal to zero. For a small Q, it is linearly proportional to Q. Hence for a exciton with small Q, we can safely neglect EXI. This allows us to calculate exciton energy spectrum and exciton wave functions, considering only the direct Coulomb interaction term.

B. Electron-hole exchange interaction description

In monolayer TMDs, the EXI couples the valley pseudospin of an exciton to its center-of-mass motion. Because of the exceptionally strong Coulomb binding of excitons in monolayer TMDs, the EXI in an exciton with a finite Q has to be accounted. Interestingly, EXI can be evaluated either numerically by TB model as displayed in the previous section (Sec. IIIA) or by the $k \cdot p$ model as shown in the following. Although the calculations in the latter is simple, the results possess a desired precision. Taking the exchange free valley exciton doublet ($|K, \mathbf{Q}\rangle$ and $|K', \mathbf{Q}\rangle$) as a basis, i.e., $|X\rangle = \alpha^K|K, Q\rangle + \alpha^{K'}|K', Q\rangle$, one can construct the matrix of exciton Hamiltonian as a 2×2 matrix:

$$\hat{H}_X(\mathbf{Q}) = \begin{bmatrix} E^{(0)}_K(\mathbf{Q}) + J_{KK}(\mathbf{Q}) & J_{KK'}(\mathbf{Q}) \\ J^*_{KK'}(\mathbf{Q}) & E^{(0)}_{K'}(\mathbf{Q}) + J_{KK}(\mathbf{Q}) \end{bmatrix}, \tag{10}$$

with the matrix elements being given by

$$\langle \tau, \mathbf{Q}|\hat{H}_X|\tau', \mathbf{Q}\rangle = E^{(0)}_\tau(\mathbf{Q})\delta_{\tau,\tau'} + J_{\tau\tau'}(\mathbf{Q}), \tag{11}$$

where $E^{(0)}_\tau(\mathbf{Q})$ is the exciton energy in the τ valley with Q momentum in the absence of EXI. The wave functions of the exchange-free exciton states in momentum space are described by

$$|\tau, \mathbf{Q}\rangle = \frac{1}{\sqrt{\mathcal{A}}}\sum_{vc\mathbf{k}} A^{(0)}_{\tau,\mathbf{Q}}(vc\mathbf{k})\hat{c}^\dagger_{c,\mathbf{k}+\mathbf{Q}}\hat{h}^\dagger_{v,-\mathbf{k}}|GS\rangle \tag{12}$$

with $|GS\rangle$ being the fully occupied VBs. $J_{\tau\tau'}(\mathbf{Q})$ in Eq. (11) are intravalley ($\tau = \tau'$) and intervalley ($\tau \neq \tau'$) EXIs, governed by

$$J_{\tau\tau'}(\mathbf{Q})$$
$$= \frac{1}{\mathcal{A}}\sum_{\substack{vc\mathbf{k} \\ v'c'\mathbf{k}'}} A^{(0)}_{\tau,\mathbf{Q}}(vc\mathbf{k})W^x_{(\mathbf{k},v,c),(\mathbf{k}',v',c'),\mathbf{Q}}A^{(0)}_{\tau',\mathbf{Q}}(v'c'\mathbf{k}'). \tag{13}$$

For $Q \to 0$, we have that $J_{K,K}(0) = J_{K',K'}(0) = J_Q$. Then the intravalley and intervalley EXI can be described by $J_Q\hat{\sigma}_0$ and $J_Q[\cos(2\phi)\hat{\sigma}_x + \sin(2\phi)\hat{\sigma}_y]$, respectively, where ϕ is the orientation angle of the center-of-mass momentum $\mathbf{Q}$ and

$$J_Q = \text{Ry}\frac{\pi}{4}\alpha^2|\psi(0)|^2\sqrt{\frac{2T_Q}{\text{Ry}}}. \tag{14}$$

In Eq. (14), α, T_Q, Ry, and $|\psi(0)|^2$ are the effective fine structure, the kinetic energy of the center-of-mass motion, the Rydberg energy, and the probability that an electron and a hole spatially overlap, respectively. They are defined by $\alpha = \frac{e^2}{\varepsilon \hbar v_F}$, $T_Q = \frac{\hbar^2 Q^2}{2M}$, $Ry = \frac{e^2}{2\varepsilon a_B}$, and $|\psi(0)|^2 \sim a_B^{-2}$ [20], with ε, a_B, M, and v_F being the environment-dependent dielectric constant, the Bohr radius, the total mass of the exciton, and the Fermi velocity, respectively. Recalling exciton binding energy $E_b = e^2/\varepsilon a_B$, the Eq. (14) can be rewritten as

$$J_Q = \frac{\pi}{8} \frac{1}{(\hbar v_F)^2} \sqrt{\frac{\hbar}{2M}} \frac{E_b^3}{\sqrt{E_b}} Q. \qquad (15)$$

After calculating the elements of the $\hat{H}_X(\mathbf{Q})$, we are ready to calculate the energies of an exciton and corresponding wave functions. Assuming that $D_{\tau,\mathbf{Q}} = E_\tau^{(0)}(\mathbf{Q}) + J_{\tau\tau}(\mathbf{Q})$, we then can rewrite Eq. (10) in a compact form as follows:

$$\hat{H}_X(\mathbf{Q}) = \bar{E}_+ \sigma_0 + \begin{bmatrix} \bar{E}_- & J_{KK'}(\mathbf{Q}) \\ J_{KK'}^*(\mathbf{Q}) & -\bar{E}_- \end{bmatrix}, \qquad (16)$$

where $\bar{E}_\pm = (D_{K,\mathbf{Q}} \pm D_{K',\mathbf{Q}})/2$. Doing algebra, we finally derive the following matrix of $\hat{H}_X$:

$$\hat{H}_X(\mathbf{Q}) = \begin{bmatrix} \bar{E}_+ + \Omega_x \cos(\theta) & \Omega_x \sin(\theta) e^{-i\phi} \\ \Omega_x \sin(\theta) e^{i\phi} & \bar{E}_+ - \Omega_x \cos(\theta) \end{bmatrix}, \qquad (17)$$

where $\Omega_x = \sqrt{\bar{E}_-^2 + |J_{KK'}(\mathbf{Q})|^2}$ and θ and ϕ are the phases in Bloch sphere, which are defined by $\theta = \cos^{-1}[\frac{\bar{E}_-}{2\Omega_x}]$ and $\phi = -\arg[J_{KK'}(Q)]$, respectively. For a special case (two degenerated valley exciton states), we have $\bar{E}_- = 0$, which corresponds to $\theta = \pi/2$. Hence only intervalley EXI impacts the exciton energy.

Diagonalizing the matrix of Hamiltonian of $\hat{H}_X(\mathbf{Q})$ in Eq. (17), we can straightforwardly obtain the eigenvalues and eigenstates of the exciton, given by $E_\pm = \bar{E}_+ \pm |J_{KK'}(\mathbf{Q})|$, and

$$|\psi_\pm\rangle = \pm e^{\pm i\phi} \sin\frac{\theta}{2} |K\rangle + \cos\frac{\theta}{2} |K'\rangle, \qquad (18)$$

where $|\psi_-\rangle$ ($|\psi_+\rangle$) represents the ground (excited) state wave function of the exciton. Thus the exciton dispersion splits into two well-separated branches by the intervalley EXI. On the boundary of the light cone, the splitting between the two branches is estimated to be a few millielectron volts. Interestingly, for this energy reference, we can rewrite the Hamiltonian in Eq. (17) as follows: $\hat{H}_Q^X = \Omega_Q^X \cdot \vec{\sigma}$, where $\vec{\sigma} = \sigma_x \hat{x} + \sigma_y \hat{y} + \sigma_z \hat{z}$ are the Pauli matrices representing valley pseudospin and $\Omega_Q^X = |J_{KK'}(\mathbf{Q})|[\sin(\theta)\cos(\phi)\hat{x} + \sin(\theta)\sin(\phi)\hat{y} + \cos(\theta)\hat{z}]$ is the effective field acting over the valley pseudospin, with $\hat{x}$, $\hat{y}$, and $\hat{z}$ being unitary vector along x, y, and z axes, respectively. In zero external magnetic field B, the exciton states are twofold degenerated. The presence of B along the z direction lifts this degeneracy, giving rise to a valley Zeeman splitting as $\Delta E_{KK'}^X = E_K^X(Q) - E_{K'}^X(Q) = g_{\text{eff}} \mu_B B$, where μ_B is the Bohr magneton and effective g factor $g_{\text{eff}} \simeq -2(g_o + 2g_s)$ with g_o and g_s denoting the orbital and spin g factors, respectively [21,22]. To visualize the orientation of valley pseudospin, we evaluate the expectation value of its components σ_x, σ_y, and σ_z in the ground state. They are governed by $\langle \bar{\sigma}_x \rangle = -\sin\theta\cos\phi$, $\langle \bar{\sigma}_y \rangle = -\sin\theta\sin\phi$, and

TABLE I. Parameters of WSe$_2$ monolayer used in our calculation. $E_\tau^{(0)}(\mathbf{Q} = 0)$ denotes the exciton energy in τ valley at $B = 0$ T and $Q = 0$. m_0 is electron mass in the vacuum and the values of g_o and g_s were adopted from Refs. [21,22].

$\hbar v_F$ (eV·Å)	3.80
M (m_0)	$0.46 + 0.42$
E_b (eV)	0.27
$E_\tau^{(0)}(\mathbf{Q} = 0)$ (eV)	1.97
g_o	2
g_s	1

$\langle \bar{\sigma}_z \rangle = -\cos\theta$. Expect, for a specific statement, the parameters used in our calculations are listed in Table I for the WSe$_2$ monolayer.

Figure 3 displays (a) exciton energies of the ground (green) and excited (violet) states and (b) energy difference ($2J_Q$) between the $|\psi_+\rangle$ and $|\psi_-\rangle$ states as a function of exciton momentum Q in the WSe$_2$ monolayer for $B = 0$ T. As expected, at $\mathbf{Q} = 0$, EXI is zero. As $\mathbf{Q}$ increases from zero, it raises linearly with Q, obeying $\Delta_{KK'} = E_+ - E_- = 2J_Q$. Expectation value of valley pseudospin $\langle \bar{\sigma}_z \rangle$ in the ground state $|\psi_-\rangle$ around $Q = 0$ for different values of magnetic field is shown in Fig. 4. We notice that at $B = 0$, the (x, y) plane pseudomagnetic field leads to an in-plane valley pseudospin, whose orientation is governed by $\langle \bar{\sigma}_z \rangle = -\cos\theta$. With increasing external magnetic field, the valley pseudospin gains out-of-plane components. Its orientation is determined by the summation of pseudomagnetic field and external magnetic field. This indicates that EXI can be effectively tuned by an external magnetic field.

IV. DISSIPATIVE DYNAMICS

The inevitable interaction of the system of interest (S) with the environment (E) gives rise to dissipative mechanisms that cause loss of coherence. Unlike a closed system, the dynamics of an open system is generally nonunitary. Within this framework, the dynamics of the reduced system S is given by the time evolution of the density matrix ρ_S, whose equation of
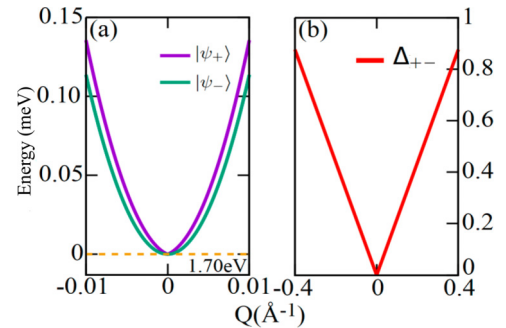
FIG. 3. (a) Exciton energies of the ground (green) and excited (violet) states in the WSe$_2$ monolayer and (b) the energy difference ($2J_Q$) between the $|\psi_+\rangle$ and $|\psi_-\rangle$ states as a function of exciton momentum Q for $B = 0$ T.
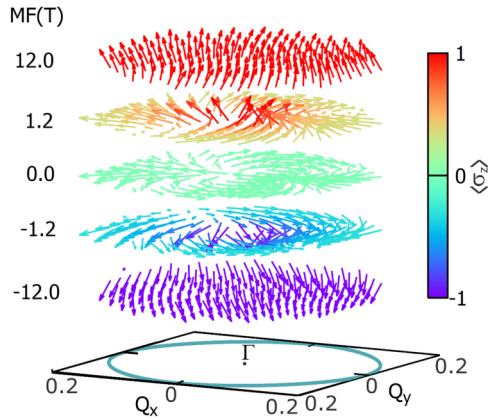
FIG. 4. Expectation value of valley pseudospin $\langle \bar{\sigma}_z \rangle$ in the ground state $|\psi_-\rangle$ around $Q = 0$ for five different values of magnetic field. The color bar indicate the value of $\langle \bar{\sigma}_z \rangle$.

motion is given by the Lindblad master equation,

$$\frac{\partial \rho_S}{\partial t} = -\frac{i}{\hbar}[H_S, \rho_S] + \mathcal{L}(\rho_S), \qquad (19)$$

where the first term represents the unitary dynamics of the system driven by the Hamiltonian H_S and the second term embraces the dissipative mechanisms written in the Born-Markov approximation. The superoperator $\mathcal{L}[\rho_S(t)]$ has a specific form for each dissipative channel, the most important being those related to radiative relaxation, decoherence of quantum superpositions, and field loss mechanisms [23]. Later, we will show the explicit forms for each of these channels.

V. SINGLE VALLEY EXCITON QUBIT IN DISSIPATIVE TMDS

In order to gain an insight into cavity promoted entanglement between two valley exciton qubits, let us examine the single exciton qubit dynamics. The optical selection rules for interband transitions allow for valley-selective excitation at the K or K' valleys using σ^+ or σ^--polarized light, respectively. Thus, near resonance, circularly polarized excitation generates a valley exciton in either the K or K' valley. Hence, in each valley, exciton can be closely described by a two-level system (TLS) where the ground state $(|0\rangle)$ is related with the exciton vacuum and the excited state $(|1\rangle)$ in which the exciton occupies the $1s$-like state. For simplicity, in the remainder of this section, we choose the K valley exciton as representative of the system. Under the excitation of a σ^+ circularly right polarized light, the Hamiltonian of the system is described by two terms,

$$H = H_X + H_{XL}. \qquad (20)$$

The first term describes the free exciton and is given by $H_X = \frac{1}{2}\hbar\omega_{10}\sigma_z$ and the second is related with the interaction of the exciton with a classical monochromatic field whose frequency ω is close to the exciton transition frequency ω_{10}. In the interaction representation and under the rotating-wave approximation (RWA), the light-matter interaction term reads,

$$H_{XL} = -\hbar(\Omega S_+ e^{-i\Delta t} + \Omega^* S_- e^{i\Delta t}), \qquad (21)$$

In Eq. (21), the strength of the field-matter interaction is given by $\Omega = \frac{\mu_{10} E_0}{\hbar}$, where μ_{10} is the transition dipole moment matrix element and E_0 the amplitude of the laser field. Also $\Delta = \omega - \omega_{10}$ is the detuning between the field and the exciton transition frequency. The transition operators are defined as $S_+ = |1\rangle\langle 0|$ and $S_- = |0\rangle\langle 1|$.

We assume to have two different dissipative channels, one due to the radiative decay and the other stemming from coherence relaxation. The former, describing the relaxation from the excited state to the ground state, is governed by the Lindblad operator $\mathcal{L}(\rho) = \frac{\Gamma}{2}(2\sigma_-\rho\sigma_+ - \sigma_+\sigma_-\rho - \rho\sigma_+\sigma_-)$, while the latter related to pure dephasing is dictated by $\mathcal{L}_{pd}(\rho) = \frac{\Gamma_{pd}}{2}(\sigma_z\rho\sigma_z - \rho)$.

An analytical solution of the dissipative dynamics can be obtained by using the unitary transformation, $\tilde{\rho}_{11} = \rho_{11}$, $\tilde{\rho}_{00} = \rho_{00}$, $\tilde{\rho}_{10} = \rho_{10}e^{-i\Delta t}$, and $\tilde{\rho}_{01} = \rho_{01}e^{i\Delta t}$. Considering the initial condition $\rho_{00}(0) = 1$ and $\rho_{11}(0) = 0$, the density matrix elements are

$$\rho_{11}(t) = \frac{R}{\Gamma + 2R}[1 - e^{-(\Gamma + 2R)t}]$$

$$\rho_{00}(t) = 1 - \rho_{11}(t)$$

$$\rho_{10}(t) = \frac{\Omega D(t)}{\Delta + i\gamma},$$

where $\gamma = \frac{1}{2}\Gamma + 2\Gamma_{pd}$, $D(t) = \rho_{11}(t) - \rho_{00}(t)$, and $R = \frac{2\gamma|\Omega|^2}{\Delta^2 + \gamma^2}$. For times longer than $t = (\Gamma + 2R)^{-1}$, the steady state is reached. The stationary population of the excited state becomes

$$\rho_{11}^{st} = \frac{|\Omega|^2}{\frac{\Gamma}{2\gamma}(\Delta^2 + \gamma^2) + 2|\Omega|^2}. \qquad (22)$$

If collisions and others sources of coherence relaxation are absent, $\gamma = \frac{\Gamma}{2}$, the population of the excited state is given by

$$\rho_{11}^{st}(\Gamma_{pd} = 0) = \frac{|\Omega|^2}{\Delta^2 + \frac{1}{4}\Gamma^2 + 2|\Omega|^2}. \qquad (23)$$

Hence the steady state is thus characterized by a dynamic equilibrium between stimulated transition and spontaneous decay.

The exciton population is shown in Fig. 5 for different sets of Hamiltonian parameters and relaxation and dephasing rates. We notice that the numerical solution is consistent with analytical data for the large time. When the system reaches steady state, they are exact equal. It confirms the validity of our numerical method. From Eq. (23), we notice that for a large detuning, $\Delta^2 \gg \Gamma^2, |\Omega|^2$ induces a small population of the excited state $\rho_{11} \sim \Omega^2/\Delta^2$. In contrast, a near-resonant strong field, $|\Omega|^2 \gg \Delta^2, \Gamma^2$ produces nearly equal populations of ground and excited states $\rho_{00} \sim \rho_{11} \sim 1/2$. For the field coupling comparable to the detuning and relaxation rate $\Omega \sim \Delta, \Gamma$, the excited state population can take appreciable values. A simple analysis of Eqs. (22) and (23) allows us to show the effect on the stationary exciton population of pure dephasing processes. For the near-resonant condition $\Delta \sim 0$, we note that if condition $2|\Omega|^2 + \Gamma^2/4 \gg \Gamma\Gamma_{pd}$ is satisfied, then the effects of pure dephasing are negligible; that is, $\rho_{11}^{st} \sim \rho_{11}^{st}(\Gamma_{pd} = 0)$. This condition is verified in monolayer TMDs, where $\Gamma_{pd} \sim 0$ [24].
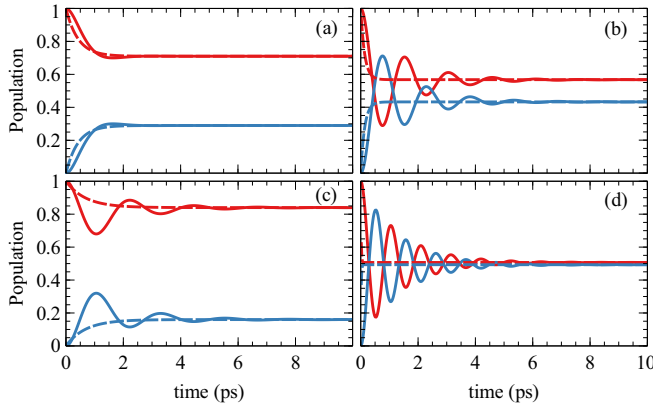
FIG. 5. Dynamics of single exciton population. Time evolution of the excited (blue) and ground (red) state populations of exciton for different values of the ratio Ω/Δ and rates Γ, Γ_{pd}. (a) $\Omega/\Delta = 1$, $\Gamma = \Gamma_{pd} = 1$ THz; (b) $\Omega/\Delta = 2$, $\Gamma = 1$ THz, $\Gamma_{pd} = 0$ THz; (c) $\Omega/\Delta = 0.5$, $\Gamma = 1$ THz, $\Gamma_{pd} = 0$ THz; and (d) resonant case $\Delta = 0$, $\Gamma = 1$ THz, $\Gamma_{pd} = 0$ THz. The solid and dashed lines correspond to the numerical data and analytical calculation, respectively.

VI. TWO VALLEY EXCITON QUBITS IN DISSIPATIVE TMDS

After understanding of single exciton qubit, we are ready to study the main features of two exciton dynamics. The system is compound by two excitons, located in the K and K' valleys. The exciton in the K valley (K') is optically driven by right (left) circularly polarized light $\sigma_+(\sigma_-)$ with frequency ω_R (ω_L). EXI mediates the intervalley coupling between the two excitons. Furthermore, an external magnetic field in the z direction acts on the bright excitons inducing a Zeeman energy, E_Z. We model the system as two TLS coupled by an exchange-like interaction, and for that we describe each exciton on the basis of excited and ground bare states as $\{|1\rangle_\tau, |0\rangle_\tau\}$, where $\tau = K, K'$. Thus, the basis on which we represent the composite system is $|1\rangle_K |1\rangle_{K'}, |1\rangle_K |0\rangle_{K'}, |0\rangle_K |1\rangle_{K'}, |0\rangle_K |0\rangle_{K'}$, which for convenience we write in the form $|11\rangle, |10\rangle, |01\rangle, |00\rangle$. The Hamiltonian of the system can be written as

$$H = H_X + H_{XL} + H_{exch}, \tag{24}$$

where the first term,

$$H_X = \sum_\tau \hbar\omega_e^\tau S_{11}^\tau,$$

describes the two noninteracting and unperturbed TLS; here the single exciton operators are $S_{11}^K = |1\rangle_K \langle 1| \otimes \mathbb{1}^{K'}$ and $S_{11}^{K'} = \mathbb{1}^K \otimes |1\rangle_{K'} \langle 1|$. Also, the energies $\hbar\omega_e^{K(K')} = E_X^{K(K')} \pm E_Z$, where $+(-)$ corresponds to $K(K')$ valley. E_X^τ are the zero-field bright τ-valley exciton energy, $E_Z = \frac{\mu}{2} g_b B$ is the Zeeman energy, μ is the Bohr magneton, and $g_b - 4.25$ is the Lande factor for WSe$_2$ bright excitons [25].

The second term of Eq. (24) accounts for the classic exciton-laser field interaction, which in RWA is given by

$$H_{XL} = \frac{\Omega_+}{2}(S_-^K \otimes \mathbb{1}^{K'})e^{i\omega_R t} + \frac{\Omega_-}{2}(\mathbb{1}^K \otimes S_-^{K'})e^{i\omega_L t} + \text{H.c.},$$

where $\Omega_\pm$ is the strength of the optical coupling for $\sigma_\pm$ polarized laser assumed here as real and H.c. denotes the Hermitian conjugate. The third term corresponds to the contribution of the EXI,

$$H_{exch} = \delta(S_+^K \otimes S_-^{K'} + S_-^K \otimes S_+^{K'}),$$

where δ is the Coulomb exchange coupling parameter. A unitary rotating frame transformation is applied on the Hamiltonian (24) designed to remove the time dependence induced by the oscillatory optical fields. The transformed Hamiltonian H' is obtained from $H' = UHU^\dagger + i\hbar \dot{U}U^\dagger$, where

$$U = e^{i(\omega_L + \frac{\omega_{RL}}{2})t}|11\rangle\langle 11| + e^{i\frac{\omega_{RL}}{2}t}|10\rangle\langle 10|$$
$$+ e^{-i\frac{\omega_{RL}}{2}}|01\rangle\langle 01| + e^{-i(\omega_L + \frac{\omega_{RL}}{2})t}|00\rangle\langle 00|,$$

and $\omega_{RL} = \omega_R - \omega_L$. The transformed Hamiltonian in the RWA approximation is given by $H' = H'_X + H'_{XL} + H'_{exch}$. The first term when $B = 0$ is

$$H_X = \Delta_K S_{11}^K + \Delta_{K'} S_{11}^{K'}, \tag{25}$$

the laser-exciton interaction is

$$H_{XL} = \frac{\Omega_+}{2}(S_-^K \otimes \mathbb{1}^{K'} + S_+^K \otimes \mathbb{1}^{K'})$$
$$+ \frac{\Omega_-}{2}(\mathbb{1}^K \otimes S_-^{K'} + \mathbb{1}^K \otimes S_+^{K'}), \tag{26}$$

and EXI is

$$H_{exch} = \frac{\delta}{2}[(S_+^K \otimes S_-^{K'})e^{-i(\Delta_K - \Delta_{K'})t} + \text{H.c.}]. \tag{27}$$

We define the energy detuning between the laser fields and excitons as $\Delta_K = E_X^K - \hbar\omega_R$, and $\Delta_{K'} = E_X^{K'} - \hbar\omega_L$, with $E_{0X}^\tau = 1.6$ eV as the zero-field exciton energy in τ valley. The experimentally accepted exchange coupling parameter for WSe$_2$ is $\delta = 0.6$ meV [26].

The system dynamics is contained in the density matrix which is obtained from the Lindblad master equation (19). Here we consider the spontaneous decay of exciton states at the rate Γ, given by

$$\mathcal{L}_{K(K')} = \mathcal{L}_X + \mathcal{L}_{XX}, \tag{28}$$

where $\mathcal{L}_X$ consider the recombination channels associated to one electron-hole pair in the K or K' valley with a rate Γ_X and $\mathcal{L}_{XX}$ represents the channel in which the two bright excitonic states recombine with a rate Γ_{XX}; this means that the biexciton state $|1\rangle_K |1\rangle_{K'}$ decays to ground state.

Writing in the product basis, this Liouville operator represents the decay between the states $|0\rangle_K |1\rangle_{K'}$, $|1\rangle_K |0\rangle_{K'}$ to ground state $|0\rangle_K |0\rangle_{K'}$ and between the states $|1\rangle_K |1\rangle_{K'}$ to states $|0\rangle_K |1\rangle_{K'}$ and $|1\rangle_K |0\rangle_{K'}$ [23]. This operator is given by

$$\mathcal{L}_X = \frac{\Gamma_X}{2}[2S_-^{K(K')}\rho S_+^{K(K')} - \rho S_+^{K(K')}S_-^{K(K')}$$
$$- S_+^{K(K')}S_-^{K(K')}\rho]. \tag{29}$$

The description of the biexciton recombination process is provided by the following equation:

$$\mathcal{L}_{XX} = \frac{\Gamma_{XX}}{2}[2(S_-^K \otimes S_-^{K'})\rho(S_+^K \otimes S_+^{K'})$$
$$- \rho(S_+^K \otimes S_+^{K'})(S_-^K \otimes S_-^{K'})$$
$$- (S_+^K \otimes S_+^{K'})(S_-^K \otimes S_-^{K'})\rho]. \qquad (30)$$

It is important to note that the biexciton decay is significantly slower than exciton recombination, and the biexciton relaxation time $\tau_{XX} = 27$ ps [27] is large in comparison with the exciton recombination time, $\tau_X \sim 1$ ps. Thus, the biexciton relaxation rate is significantly smaller than exciton decay rate, $\Gamma_{XX} \ll \Gamma_X$. Another interesting fact about dissipative dynamics in monolayer TMDs is that the mechanisms responsible for fast population relaxation do not include pure dephasing contributions [24]. Thus, pure dephasing processes as elastic exciton-exciton or exciton-phonon scattering were not considered in our calculations.

VII. CONCURRENCE BETWEEN THE VALLEY EXCITONS

Operationally, we can define entanglement through the notion of separability: a pure bipartite state $|\psi\rangle_{AB}$ is called entangled if it cannot be separated as a direct product $|\psi\rangle_{AB} = |\phi\rangle_A \otimes |\phi\rangle_B$. In the same way, a bipartite mixed state is entangled if it cannot be represented as a mixture of factorizable pure states, $\rho_{AB} = \sum_i p_i |\alpha_i\rangle \langle\alpha_i| \otimes |\beta_i\rangle \langle\beta_i|$, where $\sum_i p_i = 1$ and $|\alpha\rangle$ and $|\beta\rangle$ are the pure states of subsystems A and B, respectively. There are several approaches that provide a valid measure of entanglement. The choice of these measures depends on the nature of the physical system and the characteristics of the analysis to be performed. However, the complete quantification of quantum entanglement in the general case of multiple high-dimensional qudits is a formidable theoretical challenge that is currently under intense research.

For a simple case in which the system is composed of two exciton qubits, it is convenient to use the concurrence $\mathcal{C}(\rho)$ as a entanglement quantifier [28]. The concurrence measures the entanglement of formation of two arbitrary qubits described by the density matrix ρ and is defined by

$$\mathcal{C}(\rho) = \max(0, \sqrt{\lambda_1} - \sqrt{\lambda_2} - \sqrt{\lambda_3} - \sqrt{\lambda_4}), \qquad (31)$$

with λ_i being the eigenvalues in decreasing order of $\rho\tilde{\rho}$, where $\tilde{\rho}$ is the result of applying as the spin-flipped operation to ρ (system reduced density matrix) and $\tilde{\rho} = (\sigma_y \otimes \sigma_y)\rho^*(\sigma_y \otimes \sigma_y)$. Then the entanglement of formation of ρ can be obtained by

$$\mathcal{E}(\rho) = H\left[\frac{1 + \sqrt{1 - C^2(\rho)}}{2}\right], \qquad (32)$$

where $H(x) = -x \log_2 x - (1-x) \log_2(1-x)$ with $x > 0$. When $\mathcal{C}(\rho) = 0$, a state ρ is in a separable state. Otherwise, if $\mathcal{C}(\rho) = 1$, then it is a maximally entangled state.

VIII. RESULTS

As discussed above, TMDs exhibit rich excitonic features due to a strong Coulomb interaction. The monolayer TMDs possess a direct band gap located at the K and K' points in the first Brillouin zone. The time-reversal symmetry, the lack of inversion symmetry and the strong spin-orbit coupling lead to the splittings between opposite spin states and spin-valley locked band structure [29,30], which produces the chirality effect in the selection rules of the optical transitions. For example, the optical transitions can be selectively excited in the K (K') valleys by means of right- (left-) hand circularly polarized light. Optical interband transitions between two like-spin states in the WSe$_2$ monolayer can generate bright valley excitons in either the K or (K') valley, see Fig. 1(b). Thus, optical valley selectivity together with the intervalley coupling between two excitons in different valley induced by electron-hole exchange interaction could establish the basic architecture for applications in quantum information (QI). However, generation of entangled excitonic states which is fundamental requirement for QI applications is still a major challenge.

The generation of correlated photon pairs in structures formed by photonic crystal slabs and TMD monolayers has been successfully realized recently [31,32]. Then, one may naturally speculate that an integration of monolayer TMDs in nanocavities might also yield correlated photon states [33]. Hence the entangled stable excitonic states might be generated by virtue of the coupling of excitons with entangled quantum optical field states of an optical cavity [34–36]. In general, the creation or preservation of excitonic entanglement depends on an interplay of characteristic of the light, detuning, initial state, and the strength of EXI. Furthermore, the loss mechanisms also play an important role.

A. Valley exciton entanglement transferred from two-mode classical driving fields

To win an insight into generation of exciton entanglement, we start with our discussion about the semiclassical interaction of the composite excitonic system with circularly polarized classical field modes.

The ground and excited states of the excitonic quasiparticles in the τ valley are represented by $|i\rangle_\tau$, where $i = 0, 1$ and τ is a valley index referring to the K and K' valleys. Apart from the optical field, another important ingredient which can be used to tune the exciton entanglement is EXI δ. It mixes the two excitonic states lying in different valleys. Namely, the excitonic states $|0\rangle_K |1\rangle_{K'}$ couple with $|1\rangle_K |0\rangle_{K'}$ in such a way that the nonunitary evolution can lead the system to a partially entangled state of type $|\psi\rangle^E \sim |0\rangle_K |1\rangle_{K'} \pm |1\rangle_K |0\rangle_{K'}$. In addition, the dynamics of the exciton states is primarily governed by the exciton-field detuning, which can be partially tuned with an external magnetic field applied along the z direction. In the following, we assume that the excitonic states are driven by right- (R) and left- (L) hand circularly polarized lights with frequencies ω_R and ω_L. Furthermore, in order to measure the entanglement between two valley exciton qubits, we introduce the concurrence $\mathcal{C}(\rho)$ and evaluate it for two different initial states: a separable exciton state $|\psi_A^X\rangle = |1\rangle_K |0\rangle_{K'}$ and a maximally entangled exciton state $|\psi_B^X\rangle = \frac{1}{\sqrt{2}}(|0\rangle_K |1\rangle_{K'} - |1\rangle_K |0\rangle_{K'})$.

Figure 6 shows the time evolution of the concurrence of the exciton states driven by continuous-wave lasers. Figures 6(a)
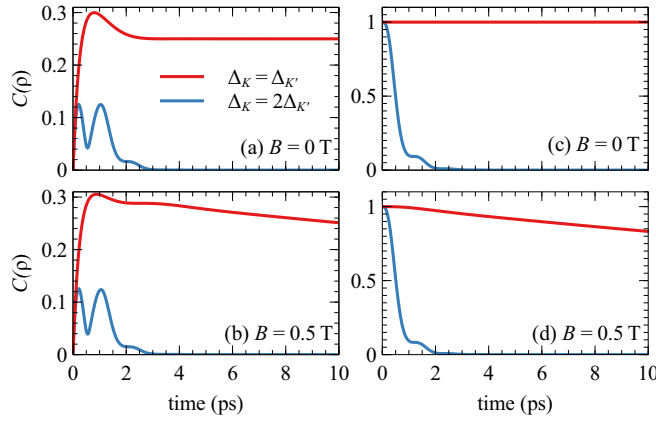
FIG. 6. Dynamics of exciton concurrence under resonant detuning ($\Delta_K = \Delta_{K'} = 7\,\text{meV}$) (red line) and nonresonant detuning ($\Delta_K = 7\,\text{meV}$, $\Delta_{K'} = 3.5\,\text{meV}$) (blue line). In panels (a) and (b), the initial state is the state $|\psi_A^X\rangle$, where the exciton states are in a product state, while panels (c) and (d) correspond to the initial state $|\psi_B^X\rangle$ in which the exciton states are written as maximally entangled state. The exciton recombination rate is $\Gamma_X = 1.0\,\text{THz}$ and exchange coupling $\delta = \delta_0 = 0.6\,\text{meV}$.

and 6(b) correspond to the concurrences of the system with exciton separable initial state ($|\Psi_A^X\rangle$), while Figs. 6(c) and 6(d) are the corresponding results of the system with maximally entangled exciton initial state ($|\Psi_B^X\rangle$), and in both cases $\delta_0 = 0.6\,\text{meV}$. In each panel, there are two curves displaying the concurrence of the system with equal exciton-field detunings in two valleys, i.e., $\Delta_K = \Delta_{K'} = 7\,\text{meV}$ (red curves), and with different detunings, i.e., $\Delta_K = 2\Delta_{K'} = 7\,\text{meV}$ (blue curves). A magnetic field effect is also exhibited, e.g., upper (lower) panels show the concurrence in the absence (presence) of the magnetic field (0.5 T). We can note that in the case of $\Delta_K \neq \Delta_{K'}$, the zero-field concurrence exhibits the same behavior with that at finite magnetic field. It drops to zero for a short time. For the system with the initial state $|\Psi_B^X\rangle$ the concurrence falls down from one to zero rapidly. In contrast, for the system with an initial state $|\Psi_A^X\rangle$, the concurrence initially increases from zero up to 0.15 and then oscillates on the picosecond timescale, and after that it goes down to zero. Although an increase of EXI (not shown here) leads to the time of the concurrence oscillation longer and the amplitude of the oscillation bigger (around 0.8), the entanglement still cannot achieve a stationary regime. On the other hand, in the case of $\Delta_K = \Delta_{K'}$, if the initial state of the system is a maximally entangled exciton state $|\Psi_B^X\rangle$, the concurrence remains constant ($\mathcal{C} = 1$). This happens because the state $|\Psi_B^X\rangle$ is an eigenstate of an exciton at $B = 0$. Since the magnetic field changes detuning via Zeeman energy, we observe that the concurrence at $B = 0.5$ is no longer stationary; instead, it decreases smoothly with time. A similar asymptotic behavior is also observed for the system with an initial state $|\Psi_A^X\rangle$. Namely, at $B = 0\,\text{T}$, the concurrence acquires a small but stationary value $\mathcal{C} \sim 0.25$. But for $B \neq 0$, it decreases with an almost constant rate. Therefore, only in the case of the detunings between the laser field energy and the transition energy of the excitons in K and K' valleys being rigorously equal can partially entangled stationary states be created.

B. Generation of maximally entangled long-lived exciton states in bimodal QED cavity

We now turn our attention on to the generation of entanglement between bright excitonic states located in different valleys coupled by two modes cavity. We consider a WSe$_2$ monolayer integrated in a bimodal optical cavity, such as a circular symmetry pillar cavity, although photonic crystal nanocavities can also be used for this purpose [37]. The Hamiltonian of the system under the RWA is described by

$$H = H_X + H_c + H_I + H_{\text{exch}}, \tag{33}$$

where the first term in Eq. (33) is the exciton Hamiltonian

$$H_X = \frac{\hbar}{2}\big[\omega_X S_{11}^K + \omega_X' S_{11}^{K'}\big], \tag{34}$$

with $\hbar\omega_X = E_{0X}^K + E_Z$ and $\hbar\omega_X' = E_{0X}^{K'} - E_Z$.

The parameters associated to physical system, such as the zero-field exciton energy, are the same as those used in the previous section. The bimodal cavity Hamiltonian is

$$H_c = \hbar\omega_a a^\dagger a + \hbar\omega_b b^\dagger b, \tag{35}$$

where the cavity modes are described by the bosonic operators a and b and the mode a (b) creates the exciton in valley $K(K')$, respectively. The each mode cavity frequency is given by ω_a and ω_b. In order to satisfy the optical selection rules, the mode a (b) is circular right (R) [left (L)] polarized. The third term of (33) is the exciton-cavity interaction written in dipole approximation,

$$H_I = g_+(a^\dagger S_-^K \otimes \mathbb{1}^{K'}) + g_-(b^\dagger \mathbb{1}^K \otimes S_-^{K'}) + \text{H.c.}, \tag{36}$$

where $g_{+(-)}$ represents the coupling strength between the bright exciton in $K(K')$ valleys with the mode cavity and H.c. denotes the Hermitian conjugate. Finally, the last term of (33) refers to the EXI between the intervalley bright excitons,

$$H_{\text{exch}} = \frac{\delta}{2}e^{-2i\theta}(S_+^K \otimes S_-^{K'}) + \frac{\delta}{2}e^{2i\theta}(S_-^K \otimes S_+^{K'}), \tag{37}$$

where θ is the $x - y$ polar angle.

The dynamics is studied by means of the density matrix operator ρ of the compound system formed by the two valley bright excitons and the two-mode cavity. Its temporal evolution is given by the Lindblad master equation obtained within the Born-Markov secular approximations (19). Here the Liouville operator $\mathcal{L} = \mathcal{L}_{K(K')} + \mathcal{L}_{\text{cav}}$ describes the incoherent contributions to the dynamics, with $\mathcal{L}_{K(K')}$ as the Lindblad operator for the exciton states (the same used to calculate the dynamics of the two exciton qubits in dissipative TMDS driven by laser fields) and $\mathcal{L}_{\text{cav}}$ the Lindblad operator for the field cavity. The total decay rate of the intensity of the cavity field at a rate κ is accounted by the term

$$\mathcal{L}_{\text{cav}} = \frac{\kappa}{2}(2a\rho a^\dagger - \rho a^\dagger a - a^\dagger a\rho)$$
$$+ \frac{\kappa}{2}(2b\rho b^\dagger - \rho b^\dagger b - b^\dagger b\rho). \tag{38}$$

To solve the master equation of the system we construct the operators in the product state basis $\{|x\rangle_K\} \otimes \{|x\rangle_{K'}\} \otimes \{|n_a\rangle\} \otimes \{|n_b\rangle\}$, where $|x\rangle_\tau$ are the exciton states and $|n_a\rangle$ ($|n_b\rangle$) is the Fock basis for the right (left) polarization mode of the cavity and $|x\rangle_\tau = |0\rangle_x$ or $|1\rangle_x$ denote the vacuum

and exciton states in the τ valley, as described before. The Fock state basis is numerically truncated when any relevant expected value no longer changes when the basis size increases by 1.

We explore the dynamics of the dissipative system in order to analyze the dynamic behavior of quantum entanglement between excitonic qubits. For this purpose, we consider two types of initial states written as a product of exciton and field initial states, $|\Psi(0)\rangle = |\psi_X(0)\rangle \otimes |\psi_f(0)\rangle$: (i) $|\Psi_A\rangle = |\psi_X\rangle \otimes |\psi_f^E\rangle$, where the exciton subsystem is in an uncorrelated state $|\psi_X\rangle = |1\rangle_K \otimes |0\rangle_{K'}$, while the field is in a linearly polarized state, which corresponds to a maximally entangled Bell state [33], $|\psi_f^E\rangle = \frac{1}{\sqrt{2}}(|0\rangle_R|1\rangle_L + |1\rangle_R|0\rangle_L)$. (ii) $|\Psi_B\rangle = |\psi_X^E\rangle \otimes |\psi_f\rangle$, where the excitons are in a partial entangled state [38] $|\psi_X^E\rangle = C_1|0\rangle_K|1\rangle_{K'} + C_2|1\rangle_K|0\rangle_{K'}$, and the field is given by a Fock product state, $|\psi_f\rangle = |0\rangle_R|1\rangle_L$. Here $|C_1|^2 + |C_2|^2 = 1$; if $B = 0$ and $E_{0X}^K = E_{0X}^{K'}$, then $C_1 = C_2 = \frac{1}{\sqrt{2}}$.

As we did in the case of two exciton qubits without cavity, we define the energy detuning between the field modes and excitons, $\Delta_K = E_{0X}^K - \hbar\omega_a$ and $\Delta_{K'} = E_{0X}^{K'} - \hbar\omega_b$. If the energies of two light modes are strictly equal, then $\Delta_K = \Delta_{K'}$. However, the imperfections of the cavity symmetry could modify the energy of the light modes, leading to a slight difference between the detunings in valley K and K', that is, $\Delta_K \neq \Delta_{K'}$.

In our system, the two exciton states are indirectly coupled via cavity field, serving as a two-qubit system. The entanglement of two qubits is quantified by means of the concurrence ($\mathcal{C}$), which can be obtained from the exciton reduced density matrix ρ_X. This density matrix carries only the dynamics of the excitons considering the effects of all interactions contained in the total Hamiltonian. We obtain ρ_X by tracing the overall system density matrix, ρ_S, over the cavity degrees of freedom, as [42]

$$\rho_X \equiv \mathrm{Tr}_c(\rho_S), \tag{39}$$

where the index c refers to cavity field variables. In order to estimate the excitonic concurrence, we must solve the Lindblad master equation, considering the full Hamiltonian (33) and the excitonic (29), (30) and cavity loss mechanisms (38). Once the multipartite density matrix $\rho_S(t)$ is obtained, we apply the partial trace operation (39) to obtain the reduced density matrix of the excitonic system, ρ_X. After that, we evaluate concurrence $\mathcal{C}[\rho_X(t)]$, which should inform us about the entanglement resulting from the multiple interactions of the excitons with the cavity quantum fields and the EXI. We also evaluate the stationary concurrence, $\mathcal{C}(t \to \infty)$, which is obtained for sufficiently long times where no temporal variation of concurrence is observed.

In order to check the validity of our calculation methodology, we have performed a numerical calculation and our model prediction reproduces the result reported in Ref. [33] (not shown here), which illustrates the dynamical emergence of maximally entangled excitonic states at well-defined times in TMD monolayers. This result is based on unitary dynamics, assuming that the initial state of the field is a Bell state ($\mathcal{C} = 1$). To reproduce this result, we switched off all
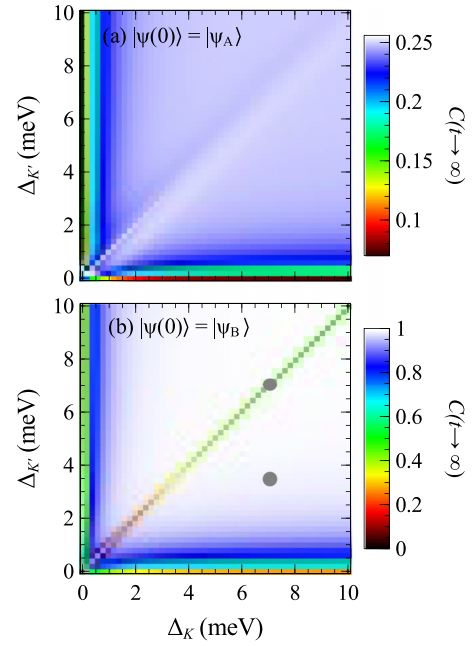
FIG. 7. Asymptotic concurrence $\mathcal{C}(t \to \infty)$ as a function of exciton-field detunings when $B = 0$ T. Panel (a) is for the initial state $|\Psi_A\rangle$. Panel (b) is for the initial state $|\Psi_B\rangle$ (see text for a description of initial states). The following parameters are used in the calculations: EXI $\delta = \delta_0 = 0.6$ meV [26,39,40], exciton-cavity modes coupling $g_+ = g_- = 0.1$ THz, and the loss rates $\Gamma_K = \Gamma_{K'} = 1$ THz [41] and $\kappa = \kappa_0 = 0.243$ THz [41]. The gray dots in (b) represent the two sets of detuning parameters $(\Delta_K, \Delta_{K'})$ used in most of the calculations.

the scattering channels which cause the decoherence of the field and excitons. Since no decoherence mechanisms were considered, we find that the concurrence oscillates periodically and reaches its maximum value at well-defined times. This behavior indicates that, in unitary dynamics, there is an effective entanglement transfer between the quantum field and the exciton subsystem. Let us demonstrate that this transfer can be effective in nonunitary dynamics as well and leads to stationary excitonic entanglement. Unless explicitly mentioned, the following parameters are used in the calculations: EXI $\delta = \delta_0 = 0.6$ meV [26,39], exciton-cavity modes coupling $g_+ = g_- = 0.1$ THz, and the loss rates $\Gamma_K = \Gamma_{K'} = 1$ THz [41] and $\kappa = \kappa_0 = 0.243$ THz [41].

The time-asymptotic stationary concurrence is showed in Fig. 7, $\mathcal{C}(t \to \infty)$ as a function of detunings Δ_K and $\Delta_{K'}$ at $B = 0$ for the two initial states [Fig. 7(a)] $|\Psi_A\rangle$ and [Fig. 7(b)] $|\Psi_B\rangle$. Two interesting features are displayed. One is the impact of the initial state on the concurrence, and the other is dependence of the concurrence on detunings $(\Delta_K, \Delta_{K'})$. For the system with a resonant detuning $(\Delta_K = \Delta_{K'})$, if the system evolves from the initial state $|\Psi_A\rangle$, then the concurrence increases initially and then oscillates with time and finally saturates at its maximum value of $\mathcal{C} \sim 0.3$. In stark contrast, if the system with an initial state $|\Psi_B\rangle$, then the concurrence has a dip at $\Delta_K = \Delta_{K'}$ and a stationary value of $\mathcal{C} \sim 0.9$ in the wide region of the figure where $\Delta_K \neq \Delta_{K'}$. The underlying physics can be understood as follows. If $\Delta_K = \Delta_{K'}$, then the coupling between the exciton and the cavity modes is optimal.
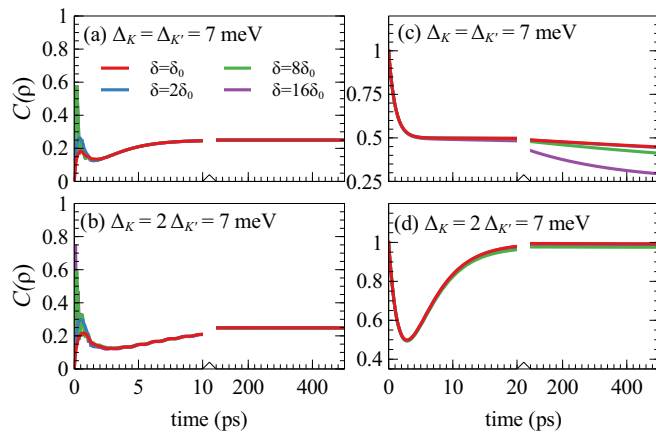
FIG. 8. Time evolution of exciton concurrence at $B = 0\,\mathrm{T}$ for different EXI strength δ. Panels (a) and (b) show the initial state $|\Psi_A\rangle$ and panels (c) and (d) show the system initially in the $|\Psi_B\rangle$ state. Upper panels show resonant detuning ($\Delta_K = \Delta_{K'}$), while the lower panels show the nonresonant detuning ($\Delta_K \neq \Delta_{K'}$).

For the system with an initial state $|\Psi_A\rangle$, the maximum entangled photon subsystem transfers part of its entanglement to the excitons, leading to an increase of exciton entanglement as well as the exciton concurrence. This behavior is more pronounced for $\Delta_K < 2$ meV. On the other hand, for the system with an initially entangled exciton state $|\Psi_B\rangle$, it might transfer a fraction of its entanglement to the photon subsystem. This causes an abrupt decrease in excitonic entanglement in the region defined by $\Delta_K = \Delta_{K'}$ where the exciton-field coupling is more efficient. The appreciable oscillation of the exciton concurrence on the picosecond timescale evidences the transference of entanglement between the two subsystems. In addition, the incoherent scattering channels causes an asymptotic behavior of the exciton populations, freezing the entanglement to the values of $\mathcal{C} < 0.3$.

Figure 8 depicts the time evolution of the concurrence of the exciton qubits for different values of the electron-hole exchange interaction strength δ. The curves in Figs. 8(a) and 8(b) are obtained assuming that the photon entangled state $|\Psi_A\rangle$ is the initial state, while Figs. 8(c) and 8(d) show the concurrences with an exciton Bell state $|\Psi_B\rangle$ as an initial state. In the former (the left panels), for the systems with resonant ($\Delta_K = \Delta_{K'}$) and nonresonant ($\Delta_K \neq \Delta_{K'}$) detunings, the concurrence does not exhibit a observable difference. EXI only plays a role at earlier stages of the concurrence dynamics. As time goes on, the concurrence evolves into a time-independent plateau due to the decoherence. In both cases, the stationary concurrence C is about 0.25. When the initial state is switched from $|\Psi_A\rangle$ to $|\Psi_B\rangle$, however, the concurrence presents a different time evolution and EXI dependence, see Figs. 8(c) and 8(d). The entanglement of exciton qubits stemming from the initial state decays rapidly in the first few picoseconds of dynamics. This behavior depends only slightly on EXI. It is attributed to the high excitonic recombination rate. Unlike the former case, shown in Figs. 8(a) and 8(b), the time evolution of the concurrence depends strongly on the detuning conditions. The behavior of the concurrence in the case shown in Fig. 8(c) draws attention. Here the initial state of

the excitons corresponds to a Bell superposition of states $|01\rangle$ and $|10\rangle$. The subspace of these states behaves as a two-level system coupled by EXI. This subspace is relevant to the dynamics of the whole system since the early stages of the time evolution are governed by EXI and the initial entangled state is essentially an eigenstate of this subspace. Exciton recombination forces the concurrence to decrease rapidly to 0.5 independent of the value of the EXI coupling. With time passing, the effective coupling between the excitonic system and the field decreases obeys the following relation $\sim \sqrt{\delta^2 + g_\pm^2}$. Thus, by increasing the EXI strength, the effective exciton-field coupling increases and the excitonic system transfers a fraction of its entanglement to the field. For $t > 5$ ps, however, the concurrence $\mathcal{C}$ decreases linearly with time with very small slope of the order of 10^{-4} for $\delta < 2\delta_0$. Hence one can approximately consider it as a stationary concurrence. Nevertheless, the strong EXI ($\delta > 2\delta_0$) changes this situation, suppressing the entanglement of the exciton qubits.

In the case of $\Delta_K \neq \Delta_{K'}$, shown in Fig. 8(d), the coupling between the excitons and the cavity field is less efficient, which disfavors the entanglement transfer from the excitons to the optical field. But the interplay of this mechanism and the large excitonic recombination rate results in a pronounced decrease of exciton entanglement within the first picoseconds. Interestingly, as time goes on further, the quantum interference governed by EXI creates a superposition of the stationary Bell-type exciton states which are eigenstates of the exciton Hamiltonian at $B = 0$. Consequently, the entanglement revives and concurrence can reach a giant value close to 1. It is interesting to recall that the entanglement transfer is damped by the cavity loss mechanisms.

Until now, we have mainly focused our attention on the concurrence of the exciton qubits in the valley degenerate states, i.e., $E_{0X}^K = E_{0X}^{K'}$, which implies that $\hbar\omega_X = \hbar\omega_X'$. As known, an external magnetic field can lift the valley degeneracy of the exciton states in TMD monolayers due to Zeeman valley splitting. This allows us to study an entanglement of two nondegenerate exciton states in the K and K' valleys. Subjected to an external magnetic field of $B = 0.5$ T along the z axis, it produces 0.12-meV valley Zeeman splitting. Although this splitting is small in comparison with other energy scales of the problem, it can induce a profound impact on the concurrence behavior. Figure 9 shows that for a moderate value of δ ($\delta < 2\delta_0$), the lifting of exciton valley degeneracy suppresses the exciton entanglement, see the red and blue curves. In addition, this behavior occurs for an experimentally accessible EXI parameter. Because breaking exciton degeneracy makes the coherent dynamics of the exciton qubits more susceptible to incoherent effects. Then the correlation between excitons induced by a weak EXI is not strong enough to bring the system to a quasistationary state and maintain the entanglement. In Figs. 9(a) and 9(b), we show time evolution of the exciton concurrence in the system with an initial state $|\Psi_A\rangle$. In contrast to Figs. 8(a) and 8(b), the concurrence is strongly dependent on exchange coupling δ. As aforementioned, for $\delta < 2\delta_0$, the concurrence decreases exponentially. For $t > 300$ ps, the degree of entanglement vanishes practically. For the large value of the EXI ($\delta > 8\delta_0$), however, the concurrence can
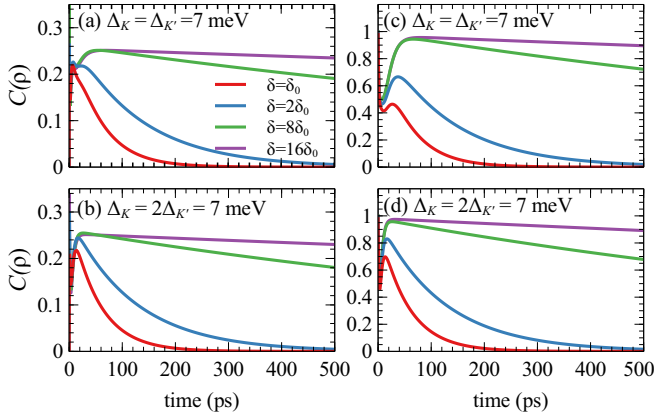
FIG. 9. Same as Fig. 8 but for $B = 0.5$ T. Curves shown in panels (a) and (b) are obtained with the initial state $|\Psi_A\rangle$, while panels (c) and (d) correspond to the initial state $|\Psi_B\rangle$. Upper panels show resonant detuning ($\Delta_K = \Delta_{K'}$), while the lower panels correspond to the nonresonant detuning ($\Delta_K \neq \Delta_{K'}$).

FIG. 10. Effects of cavity loss rate κ on the temporal evolution of concurrence of two exciton qubits in WSe$_2$ monolayer integrated to the cavity in zero (upper panels) and 0.5 T (lower pannels) vertical magnetic field for five cavity loss rates, for $\Delta_K = 7$ meV, $\Delta_{K'} = 3.5$ meV, the cavity loss rate is scaled by $\kappa = \eta\kappa_0$ with $\kappa_0 = 0.234$ THz and exchange coupling $\delta = \delta_0 = 0.6$ meV. Left panels (a) and (b) correspond to initial state $|\Psi_A\rangle$ and right panels (c) and (d) are obtained assuming the initial state $|\Psi_B\rangle$.

establishes its quasistationary value. Moreover, the behavior of the concurrence only slightly depends on the detuning δ_τ. In both resonant and nonresonant detuning cases, the asymptotic value of $\mathcal{C} \sim 0.25$ for $\delta = 16\delta_0$. Figures 9(c) and 9(d) show the concurrence of exciton qubits with the initial state $|\Psi_B\rangle$ for several δ values. For $\delta < 2\delta_0$, the initial excitonic entanglement is quickly dampened. The transference of entanglement to the field subsystem and the dissipative sources impede the system to reach its steady state. However, an enhancement of the excitonic correlation mediated by EXI causes a progressive recovery of the quasistationary behavior of the concurrence. Hence the EXI can be employed to restore exciton entanglement, independent of their detuning condition. For instance, for $\delta = 16\delta_0$, the stationary value of the concurrence reaches almost as large as 1, see Figs. 9(c) and 9(d). Since the external magnetic field lifts the degeneracy of two excitons in the K and K' valleys due to the valley Zeeman splitting, Fig. 9 shows the concurrence of the excitons in essentially nonresonant detuning condition. In this regime the system is essentially in nonresonant detuning condition, one could reasonably expect that the effect of the initial detuning condition set up by and is not relevant. Therefore the corresponding figures of the concurrence shown in Fig. 9(a) and 9(b) are similar, analogically for Fig. 9(c) and 9(d). In comparison of Fig. 8(c) with Fig. 9(c), the concurrence of two nondegenerate exciton states is quite different from that of two degenerate states. Finally, Fig. 10 depicts the effects of cavity loss rate κ on the excitonic concurrence for $\delta = \delta_0$, $\Delta_K = 7$ meV, and $\Delta_{K'} = 3.5$ meV. The results shown in the right (left) panels are obtained by assuming that the initial state is $|\Psi_A\rangle$ ($|\Psi_B\rangle$). Since the cavity field loss significantly modifies the temporal evolution of the concurrent, we use a longer timescale in this figure than that used in the previous figures. For convenience, κ is scaled with an η parameter such that $\kappa = \eta\kappa_0$. In the absence of magnetic field, the two exciton states are valley degenerate states. As time goes by, the concurrence establishes its stationary value which depends only slightly on κ in the range of approximately $(0.1 - 1)\kappa_0$. In the nondegenerate case, e.g., at $B = 0.5$ T, however, the

concurrence inevitably diminishes to zero for sufficiently long times. In addition, the smaller the cavity loss rate, the faster the concurrence approaches zero. It is interesting to recall that the rapid decay of the concurrence can be circumvented when the exchange coupling is large enough, for example, $\delta > 15\delta_0$, see Fig. 9. Therefore, cavity loss plays an important role mainly in the initial stages of the concurrence dynamics, while its stationary value is only slightly altered by cavity loss.

IX. CONCLUSION

We report the dissipative dynamics of two valley excitons residing in the K and K' valleys of WSe$_2$ monolayers, coupled by EXI, under both classical and quantum optical excitations. Entanglement between valley exciton qubits has been quantitatively measured by concurrence. It depends strongly on the nature of pumping laser. Under a classical beam excitation, the concurrence is very sensitive to the status of the detuning. For the resonant detuning, stationary concurrences are obtained. If the initial state is a maximally entangled Bell state, then a storage of the concurrence is found, i.e., it remains ~ 1. Otherwise, the system exhibits a small concurrence. For a nonresonant detuning, however, it is impossible to achieve a stationary entanglement. In contrast, under a quantum optical excitation, the transfer of entanglement from one subsystem (exciton/light) to the other (light/exciton) takes place. Hence a finite stationary concurrence is always found, independent of the detuning being whether resonant or nonresonant. Hence it is in contrast with that of classical light excitation, especially for the nonresonant detuning. In this case, while the concurrence is zero for classical beam exciton, it might be remarkably as high as 1 for quantum optical excitation. Since there is no system with a strictly resonant detuning in practice, the TMD integrated with nanocavity overcomes the challenge faced by bare TMD monolayers. Finally, the lifting of the excitonic state degeneracy induced by the magnetic

field suppresses stationary concurrence. Nevertheless it can be partially compensated by an increase of EXI.

ACKNOWLEDGMENTS

[1] J. F. Felix, A. F. da Silva, S. W. da Silva, F. Qu, B. Qiu, J. Ren, W. M. de Azevedo, M. Henini, and C.-C. Huang, A comprehensive study on the effects of gamma radiation on the physical properties of a two-dimensional WSe_2 monolayer semiconductor, Nanosc. Horiz. **5**, 259 (2020).

[2] Y. Ma, Q. Wang, S. Han, F. Qu, and J. Fu, Fine structure mediated magnetic response of trion valley polarization in monolayer WSe_2, Phys. Rev. B **104**, 195424 (2021).

[3] A. M. Jones, H. Yu, N. J. Ghimire, S. Wu, G. Aivazian, J. S. Ross, B. Zhao, J. Yan, D. G. Mandrus, D. Xiao, W. Yao, and X. Xu, Optical generation of excitonic valley coherence in monolayer WSe_2, Nat. Nanotechnol. **8**, 634 (2013).

[4] F. Qu, H. Bragança, R. Vasconcelos, F. Liu, S. Xie, and H. Zeng, Controlling valley splitting and polarization of dark-and bi-excitons in monolayer WS_2 by a tilted magnetic field, 2D Mater. **6**, 045014 (2019).

[5] D. Xiao, G.-B. Liu, W. Feng, X. Xu, and W. Yao, Coupled spin and valley physics in monolayers of MoS_2 and other group-VI dichalcogenides, Phys. Rev. Lett. **108**, 196802 (2012).

[6] M. Brooks and G. Burkard, Electric dipole spin resonance of two-dimensional semiconductor spin qubits, Phys. Rev. B **101**, 035204 (2020).

[7] G. Széchenyi, L. Chirolli, and A. Pályi, Impurity-assisted electric control of spin-valley qubits in monolayer MoS_2, 2D Mater. **5**, 035004 (2018).

[8] F. Wu, F. Qu, and A. H. MacDonald, Exciton band structure of monolayer MoS_2, Phys. Rev. B **91**, 075310 (2015).

[9] A. C. Dias, H. Bragança, H. Zeng, A. L. A. Fonseca, D.-S. Liu, and F. Qu, Large room-temperature valley polarization by valley-selective switching of exciton ground state, Phys. Rev. B **101**, 085406 (2020).

[10] M. Bieniek, M. Korkusiński, L. Szulakowska, P. Potasz, I. Ozfidan, and P. Hawrylak, Band nesting, massive Dirac fermions, and valley Landé and Zeeman effects in transition metal dichalcogenides: A tight-binding model, Phys. Rev. B **97**, 085153 (2018).

[11] C. S. Tang, X. Yin, M. Yang, D. Wu, M. D. Birowosuto, J. Wu, C. Li, C. Hettiarachchi, X. Y. Chin, Y.-H. Chang, F. Ouyang, C. Dang, S. J. Pennycook, Y. P. Feng, S. Wang, D. Chi, M. B. H. Breese, W. Zhang, A. Rusydi, and A. T. S. Wee, Three-dimensional resonant exciton in monolayer tungsten diselenide actuated by spin-orbit coupling, ACS Nano **13**, 14529 (2019).

[12] J. R. Schaibley, H. Yu, G. Clark, P. Rivera, J. S. Ross, K. L. Seyler, W. Yao, and X. Xu, Valleytronics in 2D materials, Nat. Rev. Mater. **1**, 16055 (2016).

[13] Y. Wang, L. Deng, Q. Wei, Y. Wan, Z. Liu, X. Lu, Y. Li, L. Bi, L. Zhang, H. Lu, *et al.*, Spin-valley locking effect in defect states of monolayer MoS_2, Nano Lett. **20**, 2129 (2020).

[14] A. Altıntaş, M. Bieniek, A. Dusko, M. Korkusiński, J. Pawłowski, and P. Hawrylak, Spin-valley qubits in gated quantum dots in a single layer of transition metal dichalcogenides, Phys. Rev. B **104**, 195412 (2021).

[15] N. Rohling and G. Burkard, Universal quantum computing with spin and valley states, New J. Phys. **14**, 083008 (2012).

[16] P. Giannozzi, S. Baroni, N. Bonini, M. Calandra, R. Car, C. Cavazzoni, D. Ceresoli, G. L. Chiarotti, M. Cococcioni, I. Dabo, A. D. Corso, S. de Gironcoli, S. Fabris, G. Fratesi, R. Gebauer, U. Gerstmann, C. Gougoussis, A. Kokalj, M. Lazzeri, L. Martin-Samos, N. Marzari, F. Mauri, R. Mazzarello, S. Paolini, A. Pasquarello, L. Paulatto, C. Sbraccia, S. Scandolo, G. Sclauzero, A. P. Seitsonen, A. Smogunov, P. Umari1, and R. M. Wentzcovitch, QUANTUM ESPRESSO: A modular and open-source software project for quantum simulations of materials, J. Phys.: Condens. Matter **21**, 395502 (2009).

[17] J. Heyd and G. E. Scuseria, Hybrid functionals based on a screened Coulomb potential, J. Chem. Phys. **118**, 8207 (2003).

[18] A. V. Krukau, O. A. Vydrov, A. F. Izmaylov, and G. E. Scuseria, Influence of the exchange screening parameter on the performance of screened hybrid functionals, J. Chem. Phys. **125**, 224106 (2006).

[19] A. A. Mostofi, J. R. Yates, Y.-S. Lee, I. Souza, D. Vanderbilt, and N. Marzari, An updated version of Wannier90: A tool for obtaining maximally-localised Wannier functions, Comput. Phys. Commun. **185**, 2309 (2014).

[20] H. Yu, G. B. Liu, and P. Gong, Dirac cones and Dirac saddle points of bright excitons in monolayer transition metal dichalcogenides, Nat. Commun. **5**, 3876 (2014).

[21] G. Aivazian, Z. Gong, A. M. Jones, R.-L. Chu, D. G. M. J. Yan, C. Zhang, D. Cobden, W. Yao, and X. Xu, Magnetic control of valley pseudospin in monolayer WSe_2, Nat. Phys. **11**, 148 (2015).

[22] D. S. Brandão, E. C. Castro, H. Zeng, J. Zhao, G. S. Diniz, J. Fu, A. L. A. Fonseca, C. A. N. Júnior, and F. Qu, Phonon-fostered valley polarization of interlayer excitons in van der Waals heterostructures, J. Phys. Chem. C **126**, 18128 (2022).

[23] See Supplemental Material at http://link.aps.org/supplemental/10.1103/PhysRevB.107.035404 for more details about the calculation radiative lifetime of excitons in monolayer TMD and matrix representantion of the lindblad operators.

[24] G. Moody, C. K. Dass, K. Hao, C.-H. Chen, L.-J. Li, A. Singh, K. Tran, G. Clark, X. Xu, G. Berghäuser, E. Malic, A. Knorr, and X. Li, Intrinsic homogeneous linewidth and broadening mechanisms of excitons in monolayer transition metal dichalcogenides, Nat. Commun. **6**, 8315 (2015).

[25] J. Förste, N. V. Tepliakov, S. Y. Kruchinin, J. Lindlau, V. Funk, M. Förg, K. Watanabe, T. Taniguchi, A. S. Baimuratov, and A.

Hogele, Exciton g-factors in monolayer and bilayer WSe$_2$ from experiment and theory, Nat. Commun. **11**, 4539 (2020).

[26] M. R. Molas, A. O. Slobodeniuk, T. Kazimierczuk, K. Nogajewski, M. Bartos, P. Kapuściński, K. Oreszczuk, K. Watanabe, T. Taniguchi, C. Faugeras, P. Kossacki, D. M. Basko, and M. Potemski, Probing and Manipulating Valley Coherence of Dark Excitons in Monolayer WSe$_2$, Phys. Rev. Lett. **123**, 096803 (2019).

[27] Y. You, X.-X. Zhang, T. C. Berkelbach, M. S. Hybertsen, D. R. Reichman, and T. F. Heinz, Observation of biexcitons in monolayer WSe$_2$, Nat. Phys. **11**, 477 (2015).

[28] W. K. Wootters, Entanglement of Formation of an Arbitrary State of Two Qubits, Phys. Rev. Lett. **80**, 2245 (1998).

[29] M. M. Furchi, F. Höller, L. Dobusch, D. K. Polyushkin, S. Schuler, and T. Mueller, Device physics of van der Waals heterojunction solar cells, npj 2D Mater. Appl. **2**, 3 (2018).

[30] T. Mueller and E. Malic, Exciton physics and device application of two-dimensional transition metal dichalcogenide semi-conductors, npj 2D Mater. Appl. **2**, 29 (2018).

[31] T. Wang, Improved photon-pair generation from transition-metal dichalcogenide monolayers embedded in one-dimensional photonic crystals, J. Opt. Soc. Am. A **35**, 616 (2018).

[32] T. Wang, Z. Li, and X. Zhang, Improved generation of correlated photon pairs from monolayer WSe$_2$ based on bound states in the continuum, Photon. Res. **7**, 341 (2019).

[33] M. Tokman, Y. Wang, and A. Belyanin, Valley entanglement of excitons in monolayers of transition-metal dichalcogenides, Phys. Rev. B **92**, 075409 (2015).

[34] C.-H. Liu, G. Clark, T. Fryett, S. Wu, J. Zheng, F. Hatami, X. Xu, and A. Majumdar, Nanocavity integrated van der Waals heterostructure light-emitting tunneling diode, Nano Lett. **17**, 200 (2017).

[35] Y. Li, J. Zhang, D. Huang, H. Sun, F. Fan, J. Feng, Z. Wang, and C. Z. Ning, Room-temperature continuous-wave lasing from monolayer molybdenum ditelluride integrated with a silicon nanobeam cavity, Nat. Nanotechnol. **12**, 987 (2017).

[36] L. C. Flatten, Z. He, D. M. Coles, A. A. P. Trichet, A. W. Powell, R. A. Taylor, J. H. Warner, and J. M. Smith, Room-temperature exciton-polaritons with two-dimensional WSe$_2$, Sci. Rep. **6**, 33134 (2016).

[37] C. A. Jiménez-Orjuela, H. Vinck-Posada, and J. M. Villas-Bôas, Dark excitons in a quantum-dot-cavity system under a tilted magnetic field, Phys. Rev. B **96**, 125303 (2017).

[38] The coefficients are obtained from diagonalization of bare exciton Hamiltonian $H_X = (\hbar/2)(\omega_X^K \sigma_z^K \otimes \mathbb{1}^{K'} + \omega_X^{K'} \mathbb{1}^K \otimes \sigma_z^{K'}) + \delta(S_+^K \otimes S_-^{K'} + S_-^K \otimes S_+^{K'})$, the Hamiltonian is block-diagonal in the basis space: $\{|K,0\rangle |K',1\rangle, |K,1\rangle |K',0\rangle\}$. We choose as the initial state the eigenvector $|\psi_e(0)\rangle = (C_1, C_2)^T = (\delta/R_-, -(\sqrt{\delta^2 + S^2} + S)/R_-)^T$, where $S = (E_{0X}^K - E_{0X}^{K'}) + 2E_Z$ and $R_- = [2S\sqrt{\delta^2 + S^2} + 2(\delta^2 + S^2)]^{1/2}$.

[39] C. Robert, T. Amand, F. Cadiz, D. Lagarde, E. Courtade, M. Manca, T. Taniguchi, K. Watanabe, B. Urbaszek, and X. Marie, Fine structure and lifetime of dark excitons in transition metal dichalcogenide monolayers, Phys. Rev. B **96**, 155423 (2017).

[40] C. Robert, B. Han, P. Kapuscinski, A. Delhomme, C. Faugeras, T. Amand, M. R. Molas, M. Bartos, K. Watanabe, T. Taniguchi, B. Urbaszek, M. Potemski, and X. Marie, Measurement of the spin-forbidden dark excitons in MoS$_2$ and MoSe$_2$ monolayers, Nat. Commun. **11**, 4037 (2020).

[41] A. De and R. K. Lake, Strong cavity-pseudospin coupling in monolayer transition metal dichalcogenides, Phys. Rev. B **96**, 035436 (2017).

[42] M. A. Nielsen and I. S. Chuang, *Quantum Infromation and Quantum Computation* (Cambridge University Press, Cambridge, UK, 2000).